

# Diverse and Admissible Trajectory Forecasting through Multimodal Context Understanding

Seong Hyeon Park<sup>1</sup>, Gyubok Lee<sup>2</sup>, Manoj Bhat<sup>3</sup>, Jimin Seo<sup>4</sup>, Minseok Kang<sup>5</sup>,  
Jonathan Francis<sup>3,6</sup>, Ashwin Jadhav<sup>3</sup>, Paul Pu Liang<sup>3</sup>, and Louis-Philippe  
Morency<sup>3</sup>

<sup>1</sup> Hanyang University, Seoul, Korea  
shpark@spa.hanyang.ac.kr

<sup>2</sup> Yonsei University, Seoul, Korea  
glee48@yonsei.ac.kr

<sup>3</sup> Carnegie Mellon University, Pittsburgh, PA, USA  
{mbhat, jmf1, arjadhav, pliang, lmorency}@andrew.cmu.edu

<sup>4</sup> Korea University, Seoul, Korea  
jmseo0607@korea.ac.kr

<sup>5</sup> Sogang University, Seoul, Korea  
ahstarwab@sogang.ac.kr

<sup>6</sup> Bosch Research Pittsburgh, Pittsburgh, PA, USA

**Abstract.** Multi-agent trajectory forecasting in autonomous driving requires an agent to accurately anticipate the behaviors of the surrounding vehicles and pedestrians, for safe and reliable decision-making. Due to partial observability over the goals, contexts, and interactions of agents in these dynamical scenes, directly obtaining the posterior distribution over future agent trajectories remains a challenging problem. In realistic embodied environments, each agent’s future trajectories should be *diverse* since multiple plausible sequences of actions can be used to reach its intended goals, and they should be *admissible* since they must obey physical constraints and stay in drivable areas. In this paper, we propose a model that fully synthesizes multiple input signals from the multimodal world—the environment’s scene context and interactions between multiple surrounding agents—to best model all diverse and admissible trajectories. We offer new metrics to evaluate the diversity of trajectory predictions, while ensuring admissibility of each trajectory. Based on our new metrics as well as those used in prior work, we compare our model with strong baselines and ablations across two datasets and show a **35%** performance-improvement over the state-of-the-art.

**Keywords:** Trajectory Forecasting, Diversity, Generative Modeling, Autonomous Driving, Datasets

## 1 Introduction

Trajectory forecasting is an important problem in autonomous driving scenarios, where an autonomous vehicle must anticipate the behavior of other surrounding agents (e.g., vehicles and pedestrians), within a dynamically-changing environment, in order to plan its own actions accordingly. However, since none of the goals, contexts, or interactions are directly observed, predicting future trajectories is a challenging problem [28, 35, 40]. It necessitates both the estimation of

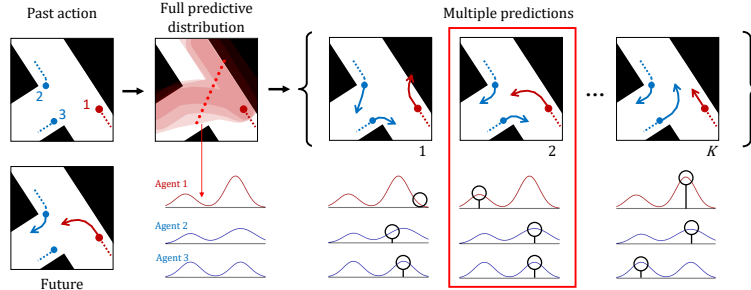


**Fig. 1.** Diverse and admissible trajectory forecasting. Based on the existing context, there can be multiple valid hypothetical futures. Therefore, the predicted future trajectory distribution should have multiple modes representing multiple plausible goals (*diversity*) while at the same time assigning low density to the implausible trajectories that either conflict with the other agents or are outside valid drivable areas (*admissibility*).

plausible agent actions based on observable environmental features (e.g., road structures, agent interactions) as well as the simulation of agents’ hypothetical future trajectories toward their intended goals. In realistic embodied environments, there are multiple plausible sequences of actions that an agent can take to reach its intended goals. However, each trajectory must obey physical constraints (e.g., Newton’s laws) and stay in the statistically plausible locations in the environment (i.e., the drivable areas). In this paper, we refer to these attributes as *diverse* and *admissible* trajectories, respectively, and illustrate some examples in Fig. 1. Achieving diverse and admissible trajectory forecasting for autonomous driving allows each agent to make the best predictions, by taking into account all valid actions that other agents could take. In addition, it allows each agent to assess the surrounding situation to ensure safety and prevent accidents.

To predict a diverse set of admissible trajectories, each agent must understand its *multimodal* environment, consisting of the scene context as well as interactions between multiple surrounding agents. While the scene context gives direct information about regions an agent can drive in, observation of other agents’ trajectories can provide additional environmental context. For example, conceptual constraints over the agent’s motion (e.g., traffic laws, road etiquette) may be inferred from the motion of the surrounding agents. Therefore, the model’s ability to extract and meaningfully represent multimodal cues is crucial.

Concurrently, another challenging aspect of trajectory forecasting lies in encouraging models to make diverse predictions about future trajectories. However, due to high-costs in data collection, most public datasets are not explicitly annotated for multiple future trajectories [8, 18, 21]. Vanilla predictive models that fit future trajectories based only on the existing annotations would severely underestimate the diversity of all possible trajectories. In addition, measuring the quality of predictions using existing annotation-based measures (e.g., displacement errors [30]) does not faithfully score diverse and admissible trajectory predictions.

As a step towards multimodal understanding for diverse trajectory forecasting, our contribution is *four-fold*.

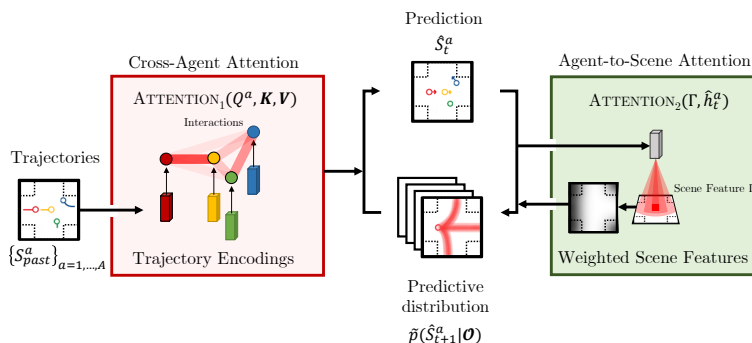


**Fig. 2.** Overview of our multimodal attention approach. Best viewed in color. The cross-agent attention module (left) generates an attention map, based on the encoded trajectories of nearby agents. The agent-to-scene attention model (right) generates an attention map over the scene, based on the posterior approximations.

1. We propose a model that addresses the lack of diversity and admissibility for trajectory forecasting through the understanding of the multimodal environmental context. As illustrated in Fig. 2, our approach explicitly models agent-to-agent and agent-to-scene interactions through “self-attention” [36] among multiple agent trajectory encodings, and a conditional trajectory-aware “visual attention” [39] over the map, respectively. Together with a constrained flow-based decoding trained with symmetric cross-entropy [27], this allows our model to generate diverse and admissible trajectory candidates by fully integrating all environmental contexts.
2. We propose a new approximation of the true trajectory distribution based on a differentiable drivable-area map. This approximation is used when evaluating our posterior likelihood. Previous approximation methods [27] utilize ground-truth (GT) trajectories to model the real distribution. However, only one GT annotation is available per agent. Our approximation method does not rely on GT samples and empirically facilitates greater diversity in the predicted trajectories while ensuring admissibility.
3. We propose a new metric, Drivable Area Occupancy (DAO), to evaluate the diversity of the trajectory predictions while ensuring admissibility. This new metric utilizes the drivable-area map, without requiring multiple annotations of trajectory futures. We couple this new metric with standard metrics from prior art, such as Average Displacement Error (ADE) and Final Displacement Error (FDE), to compare our model with existing baselines.
4. We provide a programmatic set of procedures to convert the NUSCENES [6] tracking data to a new dataset for trajectory forecasting. The procedure includes trajectory association, smoothing, imputation, and generation of the drivable-area features. These features are used for approximation of the real trajectory distribution and for calculating our new metrics. We set new state-of-the-art performance for multi-agent trajectory forecasting, wherein our model enjoys a **35%** performance-improvement over the current baselines.

We will publish tools to replicate our data and results which we hope will advance the study of diverse trajectory forecasting.

## 2 Related Work

**Multimodal trajectory forecasting** requires a detailed understanding of the agent’s environment. Many works integrate information from multiple modalities [20, 24], such as RGB image and LiDAR point-cloud information to model the surrounding environment [19, 27] and high dimensional map data to modeling vehicle lane segmentation [3, 7, 40]. Other methods additionally fuse different combinations of map context [3, 7, 10], LiDAR [19], and RGB [21, 29] with the intention of jointly capturing all interactions between the agents and environment [1, 14, 31]. Without mechanisms to explicitly model agent-to-agent and agent-to-scene interactions, we hypothesize that these models are unable to capture complex nonlinear interactions in the high-dimensional input space. In this paper, we study and propose methods to explicitly model these interactions, escalating performance in trajectory forecasting.

**Multi-agent modeling** aims to learn representations that summarize the behavior of one agent given its surrounding agents. These interactions are often modeled through either spatial-oriented methods or through neural attention-based methods. Spatial-oriented methods use pooling approaches across individual agent representations [9, 19, 40] and usually take into account inter-agent distances, through a relative coordinate system [3, 15, 22, 28]. Despite their wide usage, spatial-oriented methods are designed to concentrate only on adjacent (spatially close) agents and assume a fixed number of agents in the scene; they also limit the maximum number of agents. Attention-based methods use attention [36] architectures to model multi-agent interaction for applications involving pedestrians [12, 31, 37], sports players [11, 33], indoor robots [25], and vehicle trajectories [21, 35]. In this paper, we use a cross-agent attention module to model the agent-to-agent interaction. Rather than using this information solely for prediction, we additionally generate attended scene context, conditioned on these cross-agent representations. We hypothesize that the attended map context will lead to improved tractability in modeling high-dimensional correlations in the scene. We support this with our empirical results in Section 6.

**Diverse trajectory prediction:** Many models follow a deterministic trajectory-prediction approach [9, 40] and, therefore, struggle to estimate the diversity in the future trajectories. Some works have applied generative models such as Generative Adversarial Networks (GANs) [13, 14, 31, 40] and Variational Auto Encoders (VAEs) [19] to encourage diverse predictions. However, these approaches focus more on generating and scoring multiple output candidates and focus less on analyzing the diversity across distributional modes.

**Trajectory forecasting:** Trajectory forecasting has been studied in various domains, spanning marine vessels, aircraft, satellites, motor vehicles, and pedestrians [2, 5, 14, 28, 32]. Tasks involving motor vehicles and pedestrians are especially challenging, due to the high stochasticity that arises from attempting to model complex latent factors (e.g., human intent, “social” agent interacts, and scene context) [8]. Despite some promising empirical results, it remains difficult to evaluate both the diversity and admissibility of predictions. In this paper, we define the task of diverse and admissible trajectory forecasting and provide a new dataset generated from NUSCENES [6], a popular image tracking source. We also define new task metrics that specifically assess models on the basis of prediction

diversity and admissibility, and we analyze model generalization based on data from multiple domains.

### 3 Problem Formulation

#### 3.1 Model Architecture

We define the terminology that constitutes our problem. An *agent* is a dynamic on-road object that is represented as a sequence of 2D coordinates, i.e., a spatial position over time. We denote the position for agent  $a$  at time  $t$  as  $S_t^a \in \mathbb{R}^2$ . By writing  $S_{t_1:t_2}^a$ , we represent the sequence of its positions, between  $t_1$  and  $t_2$ .  $\mathbf{S}^a$  (bold) to denote full sequence of positions for agent  $a$ . We set  $t = 0$  as *present*,  $t \leq 0$  as *past*, and  $t > 0$  as *prediction* or simply, *pred*. We often split the sequence into two parts, with respect to the *past* and *pred* sub-sequences: we denote these as  $\mathbf{S}_{past}^a$  and  $\mathbf{S}_{pred}^a$ , respectively. A *scene* is a high-dimensional structured data that describes the present environmental context around the agent. For this, we utilize a bird’s eye view array, denoted  $\Phi \in \mathbb{R}^{H \times W \times C}$ , where  $H$  and  $W$  are the sizes of field around the agent and  $C$  is the channel size of the scene, where each channel consists of distinct information such as the drivable area, position, and distance encodings.

Combining the *scene* and all *agent* trajectories yields an *episode*. In an episode  $\mathcal{X}$ , there is a variable  $A$  number of agents, each of which plays for different time periods from between the variable *start time*  $t_s^a$  and *final time*  $t_f^a$ . As a result, the episode is the set  $\{\mathbf{S}^1, \mathbf{S}^2, \dots, \mathbf{S}^A, \Phi\}$  where  $\mathbf{S}^a \equiv S_{t_s^a:t_f^a}^a$ . In the combined setting, we often use bold  $\mathbf{S} \equiv \{\mathbf{S}^1, \mathbf{S}^2, \dots, \mathbf{S}^A\}$  to denote the agents subset of the episode  $\mathcal{X}$  and write  $\mathbf{S}_{past}$  or  $\mathbf{S}_{pred}$  to represent the set of past or pred segments of  $A$  agents. Since  $\mathbf{S}_{past}$  and  $\Phi$  serve as the observed information cue used for the prediction, they are often called *observation* simply being denoted as  $\mathcal{O} \equiv \{\mathbf{S}_{past}, \Phi\}$ . Finally, we may add the subscript  $n = 1, 2, \dots, N$  to all the notations, such as  $\mathcal{X}_n, \mathcal{O}_n, \Phi_n, S_{t,n}^a, S_{t_1:t_2,n}^a, \mathbf{S}_n^a$ , or  $\mathbf{S}_n$  to distinguish the information from different episodes.

We define *diversity* to be the level of coverage in a model’s predictions, across modes in a distribution representing all possible future trajectories. We denote the model distribution as  $q(\mathbf{S}_{pred}|\mathcal{O})$  and want the model to generate  $K$  candidates or *hypotheses*, denoted as  $\hat{\mathbf{S}}_{pred} \equiv \{\hat{\mathbf{S}}_{pred}^1, \hat{\mathbf{S}}_{pred}^2, \dots, \hat{\mathbf{S}}_{pred}^K\}$ . We interpret  $\hat{\mathbf{S}}_{pred}$  as a set of independent hypotheses that might have happened, given the same *observation*. Instead of generating samples from one mode, which we refer to as *perturbation*, we expect to build a model that generates multiple hypotheses that cover multiple modes.

Finally, we acknowledge that encouraging a model’s predictions to be diverse, alone, is not sufficient for accurate and safe output; the model predictions should lie in the support of the real future trajectory distribution  $p$ , i.e., predictions should be *admissible*. Given the observation  $\mathcal{O}$ , it is futile to predict samples around regions that are physically and statistically implausible to reach. In conclusion, our task is *diverse and admissible multi-agent motion forecasting* by modeling multiple modes in the posterior distribution over the *pred* trajectories, given the observation:  $p(\mathbf{S}_{pred}|\mathcal{O})$ .

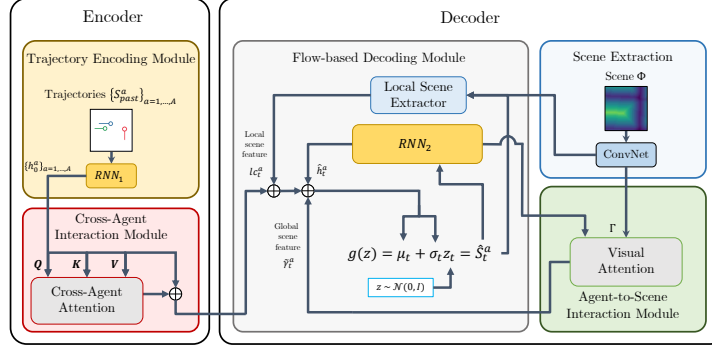


**Fig. 3.** Model Architecture. The model consists of an encoder-decoder architecture: the encoder takes as past agent trajectories and calculates cross-agent attention, and the flow-based decoder predicts future trajectories by attending scene contexts for each decoding step.

## 4 Proposed Approach

We hypothesize that future trajectories of human drivers should follow distributions of multiple modes conditioned on the scene context and social behaviors of agents. Therefore, we design our model to explicitly capture both agent-to-scene interactions and cross-agent interactions with respect to each agent of interest. Through our objective function, we explicitly encourage the model to learn a distribution with multiple modes by taking into account past trajectories and attended scene context.

As illustrated in Fig. 3, our model consists of an encoder-decoder architecture. The encoder has two modules to capture cross-agent interactions and existing trajectories. The decoder has three modules: the local scene extractor, the agent-to-scene interaction module, and the flow-based decoding module. Please refer to Fig. 4 for a detailed illustration of our main proposed modules.

The *encoder* extracts past trajectory encoding for each agent, then calculates and fuses the interaction features among the agents. Given a set of past trajectories  $\mathbf{S}_{past}$  in an observation  $\mathcal{O}$ , we encode each agent’s past trajectory  $S_{past}^a \in \mathbf{S}_{past}$  by feeding it to the agent trajectory encoding module. The module utilizes a recurrent neural network (RNN) to summarize the past trajectory. It iterates through the past trajectory with Eq. (1) and its final output  $h_0^a$  (at *present*  $t = 0$ ) is utilized as the agent embedding. Collecting the embeddings for all agents, we get  $\mathbf{h}_0 \equiv \{h_0^1, h_0^2, \dots, h_0^A\}$ . We then pass  $\mathbf{h}_0$  to the cross-agent interaction module, depicted in Fig. 4(a), which uses *self-attention* [36] to generate a cross-agent representation. We linearly transform each agent embedding to get a query-key-value triple,  $(Q^a, K^a, V^a)$ . Next, we calculate the interaction features through self-attention with  $\text{ATTENTION}_1(Q^a, \mathbf{K}, \mathbf{V})$ , where  $\mathbf{K}, \mathbf{V} \equiv \{K^1, \dots, K^A\}, \{V^1, \dots, V^A\}$ . Finally, the fused agent encoding  $\tilde{\mathbf{h}} \equiv \{\tilde{h}^1, \tilde{h}^2, \dots, \tilde{h}^A\}$  is calculated by adding the features to each agent embedding (see Eq. (2) and Fig. 4(b)). The architectural details of the encoder, which include the parameters for the agent encoding RNN and the

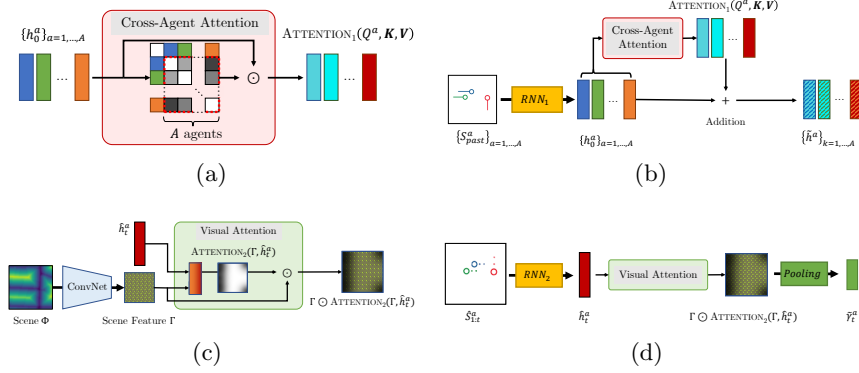


**Fig. 4.** (a) Cross-agent attention. Interaction between each agent is modeled using attention, (b) Cross-agent interaction module. Agent trajectory encodings are corrected via cross-agent attention. (c) Visual attention. Agent-specific scene features are calculated using attention. (d) Agent-to-scene interaction module. Pooled vectors are retrieved from pooling layer after visual attention.

cross-agent attention structures, are given in the supplemental material.

$$h_t^a = \text{RNN}_1(S_{t-1}^a, h_{t-1}^a) \quad (1)$$

$$\tilde{h}^a = h_0^a + \text{ATTENTION}_1(Q^a, \mathbf{K}, \mathbf{V}) \quad (2)$$

The *decoder* takes the final encodings  $\tilde{\mathbf{h}}$  and the scene context  $\Phi$  as inputs. We first extract the scene feature through a *ConvNet*,  $\mathbf{\Gamma} = \text{CNN}(\Phi)$ . The decoder then autoregressively generates the future position  $\hat{S}_t^a$ , while referring to both the local scene context  $\gamma_t^a$  and the global scene context  $\tilde{\gamma}_t^a$  from the agent-to-scene interaction module. The local scene feature  $\gamma_t^a$  is gathered using bilinear interpolation on  $2 \times 2$  crop of  $\mathbf{\Gamma}$  corresponding to the physical position  $\hat{S}_{t-1}^a$ . Then, the feature is concatenated with the encoding  $\tilde{h}^a$  and processed through fully-connected layers to make the “local context”  $lc_t^a$ . We call this part the local scene extractor. The global scene feature  $\tilde{\gamma}_t^a$  is calculated using *visual-attention* [39] to generate weighted scene features, as shown in Fig. 4(c). To calculate the attention, we first make the encoding of the previous outputs  $\hat{S}_{1:t-1}^a$ , using a RNN in Eq. (3), whose output— $\hat{h}_t^a$ —is used to calculate the pixel-wise attention at each decoding step, for each agent; the global scene feature  $\tilde{\gamma}_t^a$  (1D vector) is gathered by pooling (pixel-wise sum) the attended feature map as described in Eq. (4) and Fig. 4(d). Finally,  $\tilde{\gamma}_t^a$ ,  $\hat{h}_t^a$ , and  $lc_t^a$  are concatenated to make the “global context”  $gc_t^a$  in Eq. (5).

$$\hat{h}_t^a = \text{RNN}_2(\hat{S}_{1:t-1}^a, \hat{h}_{t-1}^a) \quad (3)$$

$$\tilde{\gamma}_t^a = \text{POOL}(\mathbf{\Gamma} \odot \text{ATTENTION}_2(\hat{h}_t^a, \mathbf{\Gamma})) \quad (4)$$

$$gc_t^a = \text{CONCAT}(\tilde{\gamma}_t^a, \hat{h}_t^a, lc_t^a) \quad (5)$$

The flow-based decoding module generates the future position  $\hat{S}_t^a$ . The module utilizes *Normalizing Flow* [26], a generative modeling method based on a bijective

and differentiable mapping. In particular, we choose an autoregressive design [17, 27, 28]. We use fully-connected layers to project the global context  $gc_t^a$  down to a 6-dimensional vector, and we split it into a vector  $\hat{\mu}_t \in \mathbb{R}^2$  and a matrix  $\hat{\sigma}_t \in \mathbb{R}^{2 \times 2}$ . Next, we transform a standard Gaussian sample  $z_t \sim \mathcal{N}(\mathbf{0}, I) \in \mathbb{R}^2$ , by the bijective and differentiable mapping  $g(z_t; \mu_t, \sigma_t) = \sigma_t \cdot z_t + \mu_t = \hat{S}_t^a$ . The “hats” in  $\hat{\mu}_t$  and  $\hat{\sigma}_t$  are removed, in order to note that they went through the following details. To ensure the positive definiteness, we apply matrix exponential  $\sigma_t = \text{expm}(\hat{\sigma}_t)$  using the formula in [4]. Also, to improve the the physical *admissibility* of the prediction, we apply the constraint  $\mu_t = \hat{S}_{t-1}^a + \alpha(\hat{S}_{t-1}^a - \hat{S}_{t-2}^a) + \hat{\mu}_t$ , where  $\alpha$  is a model degradation coefficient. When  $\alpha = 1$ , the constraint is equivalent to *Verlet integration* [38], used in some previous works [27, 28], which gives the a perfect constant velocity (CV) prior to the model. However, we found empirically that, the model easily overfits to the dataset when the the perfect CV prior is used, and perturbing the CV prior model with  $\alpha$  prevents overfitting. We use  $\alpha = 0.5$  in our model and an analysis on the effect of the degradation coefficient  $\alpha$  is given in the supplemental material.

Iterating the autoregressive decoding procedure, we get the future trajectory prediction  $\hat{S}_{\text{pred}}^a$  for each agent. Note that by sampling multiple instances of  $z_{\text{pred}}$ , we can generate the multiple future  $\hat{S}_{\text{pred}}^{k,a}$ .

#### 4.1 Drivable Area Map and Approximating P

In this work, we generate a binary mask feature of size  $\mathbb{R}^{H \times W}$  that denotes the drivable spaces around the agents. We call the feature *drivable area map* and utilize it for three different purposes: 1) deriving the approximated true trajectory distribution  $\tilde{p}$ , 2) calculating the diversity and admissibility measures, and 3) building the scene context input  $\Phi$  for the model.

Particularly,  $\tilde{p}$  is a key component for the evaluation of  $H(q, p)$  in our training objective, Eq. (7). Since  $H(q, p)$  penalizes the predicted trajectories with respect to the real distribution, the approximation should not underestimate some region of the real distribution, or diversity in the prediction could be erroneously penalized. Previous works on deriving  $\tilde{p}$  utilized the ground-truth (GT) trajectories to model the true distribution  $p$  [27]. However, there is often only one GT annotation available in datasets and the approximation based on the GT might severely assign low probability around some region in  $p$ . To cope with such problem in the previous methods, we propose a new method to derive  $\tilde{p}$  using the drivable area. Our  $\tilde{p}$  is defined based on the assumptions that every location on the drivable-area is equally probable for future trajectories to appear in and that the locations on non-drivable area are increasingly less probable, proportional to the distance from the drivable area. To derive it, we first apply the distance transform on the drivable area map, to encode the distance on each non-drivable location. Lastly, we apply softmax over the entire map to constitute it as a probability distribution. The visualizations of the  $\tilde{p}$  are available in Fig. 7. Procedures regarding the diversity and admissibility measure will be discussed in Section 5.3; details on deriving  $\tilde{p}$  and the scene context input  $\Phi$ , as well as additional visualizations and qualitative results, are given in the supplemental material.

## 4.2 Learning

Our model learns to predict the joint distribution over the future trajectories of the agents present in a given episode. In detail, we focus on predicting the conditional distribution  $p(\mathbf{S}_{\text{pred}}|\mathcal{O})$  where the future trajectory  $\mathbf{S}_{\text{pred}}$  depends on the set of observations of the past trajectories and the scene context  $\mathcal{O} \equiv \{\mathbf{S}_{\text{past}}, \Phi\}$  given an episode. As described in the previous sections, our model utilizes a bijective and differentiable mapping, parameterized by a learnable parameter  $\theta$ ,  $S_{\text{pred}}^a = f_{\theta}(z \sim q_0; \mathcal{O})$  between the future trajectory and a Gaussian prior  $q_0$  to generate and evaluate the future trajectory. Such technique, commonly aliased ‘normalizing flow’, enables our model not only to generate multiple candidate samples of future, but also to evaluate the ground-truth trajectory according to the predicted distribution  $q_{\theta}$  by using the change-of-variable formula in Eq. (6).

$$q_{\theta}(S_{\text{pred}}^a|\mathcal{O}) = q_0(f^{-1}(S_{\text{pred}}^a)) \left| \det(\partial S_{\text{pred}}^a / \partial (g^{-1}(S_{\text{pred}}^a))) \right|^{-1} \quad (6)$$

As a result, our model can simply learn to close the discrepancy between the predicting distribution  $q_{\theta}$  and the real world distribution  $p$ . In particular, we choose to minimize the combination of forward and reverse cross-entropy  $H(p, q)$  and  $H(q, p)$ , also known as ‘symmetric cross-entropy’, between the two distributions in Eq. (7) by optimizing our model parameter  $\theta$ . Minimizing symmetric cross-entropy allows model to learn generating diverse and plausible trajectory, which is mainly used in [27].

$$\min_{\theta} H(p, q_{\theta}) + \beta H(q_{\theta}, p) \quad (7)$$

To realize this, we gather the ground-truth trajectories  $\mathbf{S}$  and scene context  $\Phi$  from the dataset  $\mathcal{D}$  that we assume to well reflect the real distribution  $p$ , then optimize the model parameter  $\theta$  such that 1) the density of the ground-truth future trajectories on top of the predicted distribution  $q_{\theta}$  is maximized and 2) the density of the predicted samples on top of the real distribution  $p$  is also maximized as described in Eq.( 8).

$$\min_{\theta} \mathbb{E}_{\mathbf{S}, \Phi \sim \mathcal{D}} \left[ \mathbb{E}_{S_{\text{pred}}^a \in \mathbf{S}} - \log q_{\theta}(S_{\text{pred}}^a|\mathcal{O}) + \beta \mathbb{E}_{\hat{S}_{\text{pred}}^a \sim q_{\theta}} - \log p(\hat{S}_{\text{pred}}^a|\mathcal{O}) \right] \quad (8)$$

Such symmetric combination of the two cross-entropy guides our model to predict  $q_{\theta}$  that covers all plausible modes in the future trajectory while penalizing the bad samples that are less likely under the real distribution  $p$ . However, one major problem inherent in this setting is that we cannot actually evaluate  $p$  in practice. To cope with the problem, several ways of approximating  $p$  by using a separate model  $\tilde{p}$  have been suggested so far [27]. In this paper, we propose a new way of modeling  $\tilde{p}$  which approximates  $p$  using a discrete grid map derived from the differentiable drivable area map in our dataset which considers every drivable region around the ego-vehicle to be equally probable that the future trajectories are placed. The details about our new  $\tilde{p}$  is included in the supplemental material. Applying bilinear interpolation around each prediction time-step in the generative sample  $\hat{S}_{\text{pred}}^a$ , we get the evaluation  $\tilde{p}(\hat{S}_{\text{pred}}^a|\mathcal{O})$  that is differentiable with respect to the model parameter  $\theta$ . Our overall loss function is:

$$\frac{1}{\sum_{n=1}^N A(n)} \sum_{n=1}^N \sum_{a=1}^{A(n)} \left[ -\log q_{\theta}(S_{\text{pred},n}^a|\mathcal{O}_n) + \beta \frac{1}{K} \sum_{k=1}^K -\log p(\hat{S}_{\text{pred},n}^{a,k}|\mathcal{O}_n) \right], \quad (9)$$

where  $N$  is the batch size,  $A(n)$  is the number of total agents in  $n$ th episode, and  $K$  is the number of candidates to sample per agent. Since this objective is fully differentiable with respect to the model parameter  $\theta$ , we train our model using Adam optimizer [16], a popular variant of the stochastic gradient descent algorithm. We also use adaptive learning rate scheduling and early stopping. Optimization details are included in the supplementary.

## 5 Experimental Setup

The primary goal in the following experiments is to evaluate our model, baselines, and ablations on the following criteria- 1. Leveraging mechanisms that explicitly model agent-to-agent and agent-to-scene interactions (experiment 1 and 2). 2. Producing diverse trajectory predictions, while obeying admissibility constraints on the trajectory candidates given different approximation methods for the true trajectory distribution  $p$  (experiment 3). 3. Remaining robust to an increasing number of agents in the scene (agent complexity; experiment 4). 4. Generalizing to other domains (experiment 5). We implement all models in PyTorch [23] trained on NVIDIA TITAN X GPUs. Procedural, architectural, and training details are included in the supplementary material.

### 5.1 Dataset

Most current autonomous driving trajectory forecasting datasets are insufficient for evaluating predictions, due to the small size and the limited number of multimodal cues [21].

The ARGOVERSE motion forecasting dataset consists of a large volume of forecasting data with drivable area annotations, but lacks certain modalities i.e LiDAR point-clouds and map images. We have generated motion forecasting datasets from NUSCENES and ARGOVERSE tracking dataset using their original annotations through programmatic trajectory association, smoothing, and imputation. Unlike the ARGOVERSE forecasting dataset, this new dataset provides additional context information from LiDAR point-clouds and map information, for better forecasting performance. We utilize the trajectory record, vectorized geometry, and drivable area annotation as modalities for our research. In order to make the experimental setup of NUSCENES similar to ARGOVERSE, we crop each sequence to be 5 seconds long in total; 3 seconds for prediction and 2 seconds for observation, with a sampling rate of 2 Hz. Background information relating to NUSCENES, ARGOVERSE trajectory data generation are included in the supplementary material. By evaluating baselines and our models on both real world datasets, we provide complementary validation of each model’s diversity, admissibility, and generalizability across domains. Data extraction procedures and quantitative results on the simulated data are discussed in the supplementary material.

### 5.2 Baseline Models

**Deterministic baselines:** We compare three deterministic models with our approach, to examine our model’s ability to capture agent-to-agent interaction: *LSTM-based encoder-decoder* [34] (LSTM), *convolutional social pooling LSTM* (CSP) [9], and a deterministic version of *multi-agent tensor fusion* (MATF-D) [40]. For our deterministic model, we use an LSTM with our cross-agent

attention module in the encoder, which we refer to as the *cross-agent attention model* (CAM). Because each model is predicated on an LSTM component, we set the capacity to be the same in all cases, to ensure fair comparison.

### 5.3 Metrics

**Measuring diversity and admissibility:** We define multiple metrics that provide a thorough interpretation about the behavior of each model in terms of precision, diversity, and admissibility. For the  $i$ -th trajectory, we first evaluate a prediction in terms of Euclidean errors: *average displacement error*  $\text{ADE}^{(i)} = \frac{1}{T} \sum_{t=1}^T \|S_t^i - \hat{S}_t^i\|_2$  and *final displacement error*  $\text{FDE}^{(i)} = \|S_{t_f}^i - \hat{S}_{t_f}^i\|_2$ , or **ERROR** to denote both. To evaluate  $N$  predictions (i.e., precision), we use the average and the minimum **ERRORS**:  $\text{AVGERROR} = \frac{1}{N} \sum_{i=1}^N \text{ERROR}^{(i)}$  and  $\text{MINERROR} = \min\{\text{ERROR}^{(1)}, \dots, \text{ERROR}^{(N)}\}$ . A large **AVGERROR** implies that predictions are spread out, and a small **MINERROR** implies at least one of predictions has high precision. From this observation, we define new evaluation metrics that capture diversity in predictions: the ratio of **AVGADE** to **MINADE** and **AVGFDE** to **MINFDE**, namely **RA** and **RF**. In particular, **RF** is robust to the variability of magnitude in velocity in predictions because high **AVGADE** and high **MINADE** caused by large magnitudes will be offset and only the directional variability will remain. As a result, **RF** provides a handy tool that can distinguish between predictions with multiple modes (diversity) and predictions with a single mode (perturbation). For deterministic models, **RA** and **RF** have a value of 1.

$$\text{Ratio of AVGFDE to MINFDE (RF)} = \frac{\text{AVGFDE}}{\text{MINFDE}} \quad (10)$$

$$\text{Drivable Area Occupancy (DAO)} = \frac{\text{count}(\text{traj}_{\text{pix}})}{\text{count}(\text{driv}_{\text{pix}})} \quad (11)$$

We also report performance on additional metrics that are designed to capture diversity and admissibility in predictions. We follow [8] in the use of *Drivable Area Count* (DAC),  $\text{DAC} = \frac{n-m}{n}$ , where  $m$  is the number of predictions that go out of the drivable area and  $n$  is the total number of predictions. Next, we propose a new metric, *Drivable Area Occupancy* (DAO), which measures the percentage of pixels that predicted trajectories occupy in the drivable area. Shown in Eq. (11),  $\text{count}(\text{traj}_{\text{pix}})$  is the number of pixels occupied by predictions and  $\text{count}(\text{driv}_{\text{pix}})$  is the total number of pixels of the drivable area, both within a pre-defined grid around the ego-vehicle. Due to the nature of DAO and DAC, the number of trajectory hypotheses should be set equally for fair comparison of models.

We use **RF**, **DAO**, and **DAC** to assess the diversity and admissibility of models. Initially, **DAO** may seem like a reasonable standalone measure of both diversity and admissibility, as it only cares about diversity in a reasonable region of interest. However, **DAO** itself cannot distinguish between *diversity* (Section 3) and arbitrary stochasticity in predictions, as illustrated by Case 1 in Fig. 5: although **DAO** measures of both predictions are equal, the causality behind each prediction is different and we must distinguish the two. **RF** and **DAO** work in a complementary way and we, therefore, use both for measuring diversity. To assure the *admissibility* of predictions, we use **DAC** which explicitly counts off-road

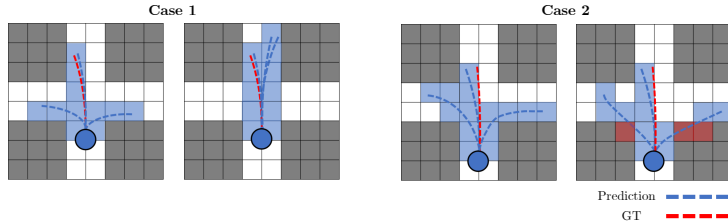


**Fig. 5.** We motivate the need for multiple metrics, to assess diversity and admissibility. Case 1: DAO measures are equal, even though predictions have differing regard for the modes in the posterior distribution. Case 2: RF measures are equal, despite differing regard for the cost of leaving the drivable area. In both cases, it is important to distinguish between conditions—we do this by using DAO, RF, and DAC together.



**Fig. 6.** Metric quality spectrum. Our newly proposed metrics: RF measures the spread of predictions in Euclidean distance, DAO measures diversity in predictions that are only admissible. DAC measures extreme off-road predictions that defy admissibility.

**Table 1.** Deterministic models on nuScenes. Our proposed model outperforms the existing baselines.

Model	MINADE ( $\downarrow$ )	MINFDE ( $\downarrow$ )
LSTM	1.186	2.408
CSP [9]	1.390	2.676
MATF-D [40]	1.261	2.538
CAM (ours)	<b>1.124</b>	<b>2.318</b>

predictions, as shown by Case 2 in Fig. 5. As a result, assessing predictions using DAO along with RF and DAC provides a holistic view of the quantity and the quality of diversity in predictions; the characteristics of each metric is summarized in Fig. 6.

For our experiments, we use MINADE and MINFDE to measure *precision*, and use RF, DAC, and DAO to measure both *diversity* and *admissibility*. Due to the nature of DAO, where the denominator in our case is the number of overlapping pixels in a  $224 \times 224$  grid, we normalize it by multiplying by 10,000 when reporting results. For the multi-agent experiment (experiment 4), relative improvement (RI) is calculated as we are interested in the relative improvement as the number of agents increases. If not specified, the number of hypotheses are set to 12 and MINFDE is reported for the performance.

## 6 Results and Discussion

In this section, we show experimental results on numerous settings including the comparison with the baseline, and ablation studies of our model. We first show the effect of our cross-agent interaction module and agent-to-scene interaction module on the model performance, then we analyze the performance with respect to different numbers of agents, and other datasets. All experiments are measured with MINADE, MINFDE, RF, DAC, and DAO for holistic interpretation.

**Effectiveness of cross-agent interaction module:** We show the performance of one of our proposed models CAM, which utilizes our cross-agent attention

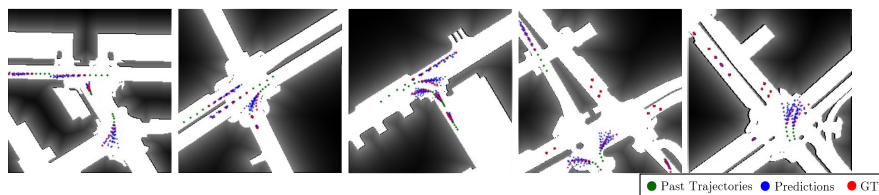


**Fig. 7.** Our map loss and corresponding model predictions. Each pixel on our map loss denotes probability of future trajectories; higher probability values are represented by brighter pixels. Our approach generates diverse and admissible future trajectories. More visualizations of qualitative results are provided in the supplementary material.

**Table 2.** Stochastic models on NUSCENES. \*\*: unstable outputs observed on R2P2-MA.

Model	MINADE ( $\downarrow$ )	MINFDE ( $\downarrow$ )	Rf ( $\uparrow$ )	DAO ( $\uparrow$ )	DAC ( $\uparrow$ )
DESIRE [19]	0.937	1.808	1.754	9.430	0.376
MATF-GAN [40]	1.053	2.124	1.194	5.950	0.391
R2P2-MA [27]	1.185	2.215	1.611	13.50**	0.396
CAM-NF (ours)	0.756	1.386	2.113	11.70	<b>0.400</b>
LOCAL-CAM-NF (ours)	0.772	1.404	2.066	11.70	<b>0.400</b>
GLOBAL-CAM-NF (ours)	0.744	1.359	2.103	11.60	<b>0.400</b>
ATTGLOBAL-CAM-NF (ours)	<b>0.638</b>	<b>1.171</b>	<b>2.558</b>	<b>12.28</b>	0.399

module, along with three deterministic baselines as shown in Tables 1. For each model we test, agent-to-agent interaction is considered in different ways. CSP models the interaction through layers of convolutional networks, and the interaction is implicitly calculated within the receptive field of convolutional layers. MATF-D is an extension of convolutional social pooling with scene information. CAM explicitly defines the interaction between each agent by using attention. The result shows that CAM outperforms other baselines in both MINADE and MINFDE, indicating that the explicit way of modeling agent-to-agent interaction performs better in terms of precision than an implicit way of modeling interaction using convolutional networks used in CSP and MATF-D. Interestingly, CAM outperforms MATF-D that utilizes scene information. This infers that our cross-agent interaction module has the ability to learn the geometric structure of the roads given by the trajectories of surrounding agents.

**Effectiveness of agent-to-scene interaction module:** The performance of stochastic models is compared in Tables 2. We experiment with removing scene processing operations in the decoder to validate the importance of our proposed agent-to-scene interaction module. As mentioned previously, generating multiple modes of sample requires a strong scene processing module and a diversity-oriented decoder. Our proposed models all outperform other stochastic baseline models in terms of precision. MATF-GAN has a small Rf inferring that the predictions are mostly unimodal, while other models such as VAE-based model DESIRE and flow-based models R2P2 and OURS show more spread in their predictions. We note that R2P2 was not designed for multi-agent setting which causing it to make unreasonably shaking outputs. Our model has the highest *DAC* and *DAO*, indicating that our models exhibit diverse and admissible predictions by accurately utilizing scene context.

**Table 3.** Optimizing using  $p$  loss outperforms MSE loss on nuScenes.

Model	MINADE ( $\downarrow$ )	MINFDE ( $\downarrow$ )	rF ( $\uparrow$ )	DAO ( $\uparrow$ )	DAC ( $\uparrow$ )
ATTGLOBAL-CAM-NF(MSE)	0.763	1.390	2.009	12.09	<b>0.400</b>
ATTGLOBAL-CAM-NF	<b>0.638</b>	<b>1.171</b>	<b>2.558</b>	<b>12.28</b>	0.399

**Table 4.** Multi-agent experiments on NUSCENES (MINFDE). RI denotes ratio of MINFDE for 10 vs. 1 agent. Our approach best models multi-agent interactions.

Model	1 agent	3 agents	5 agents	10 agents	RI(1-10)
LSTM	2.736	2.477	2.442	2.268	17.1%
CSP [9]	2.871	2.679	2.671	2.569	10.5%
DESIRE [19]	2.150	1.846	1.878	1.784	17.0%
MATF GAN [40]	2.377	2.168	2.150	2.011	15.4%
R2P2-MA [27]	2.227	2.135	2.142	2.048	8.0%
ATTGLOBAL-CAM-NF (OURS)	<b>1.278</b>	<b>1.158</b>	<b>1.100</b>	<b>0.964</b>	<b>24.6%</b>

**Table 5.** Results of baseline models and our proposed model. LOCAL-CAM-NF is an ablation, whereas ATTGLOBAL-CAM-NF is our full proposed model. The metrics are abbreviated as follows: MINADE(**A**), MINFDE(**B**), rF(**C**), DAO(**D**), DAC(**E**). Improvements indicated by arrows. \*: larger is better, as long as **A** and **B** are small.

Model	ARGOVERSE					NUSCENES				
	A ( $\downarrow$ )	B ( $\downarrow$ )	C ( $\uparrow$ )*	D ( $\uparrow$ )*	E ( $\uparrow$ )*	A ( $\downarrow$ )	B ( $\downarrow$ )	C ( $\uparrow$ )*	D ( $\uparrow$ )*	E ( $\uparrow$ )*
LSTM	1.441	2.780	1.000	1.786	0.378	1.186	2.408	1.000	1.690	0.391
CSP	1.385	2.567	1.000	1.799	0.379	1.390	2.676	1.000	1.710	0.388
MATF-D	1.344	2.484	1.000	1.768	0.379	1.261	2.538	1.000	1.690	0.384
DESIRE	0.777	1.276	<b>3.642</b>	11.80	0.301	0.937	1.808	1.754	9.430	0.376
MATF-GAN	1.214	2.316	1.099	6.075	0.376	1.053	2.124	1.194	5.950	0.391
R2P2-MA	1.270	2.190	1.589	<u>18.10</u> **	0.381	1.185	2.215	1.611	<u>13.50</u> **	0.396
CAM	1.131	2.504	1.000	1.750	<b>0.389</b>	1.124	2.318	1.000	1.670	<b>0.404</b>
CAM-NF	0.852	1.347	2.763	<b>17.60</b>	0.378	0.756	1.386	2.113	11.70	0.400
LOCAL-CAM-NF	0.807	1.250	2.858	17.00	0.381	0.772	1.404	2.066	11.70	0.400
GLOBAL-CAM-NF	0.807	1.241	3.068	16.90	0.380	0.744	1.359	2.103	11.60	0.400
ATTGLOBAL-CAM-NF	<b>0.731</b>	<b>1.126</b>	3.278	15.50	0.383	<b>0.638</b>	<b>1.171</b>	<b>2.558</b>	<b>12.28</b>	0.399

**Effectiveness of new  $p$  loss:** We experiment with MSE and our drivable area-based approximation of  $p$  in Table 3. Using our map loss in training shows superior results in most of the reported metrics. In particular, the precision and the diversity of predictions increases drastically as reflected in MINERROR and rF while DAC remains unchanged. Our map loss assures admissibility while improving precision and diversity, as drivable-area associated  $\tilde{p}$  provides additional possible regions of future trajectories.

**Complexity from number of agents:** We experiment with varying number of surrounding agents as shown in Table 4. Throughout all models, the performance increases as the number of agents increases even though we observe that many agents in the surrounding do not move significantly. In terms of relative improvement RI, as calculated between 1 agent and 10 agents, our model has the most improvement, indicating that our model makes the most use of the fine-grained trajectories of surrounding agents to generate future trajectories.

**Generalizability across datasets:** We further compare our model with baselines extensively across two more real world datasets: NUSCENES and ARGVERSE to test generalization to different environments. We show results in Table 5 where we outperform or achieve comparable results as compared to the baselines. For ARGVERSE, we additionally outperform MFP3 [35] in MINFDE with 6 hypotheses: our full model shows a MINFDE of 0.915, while MFP3 achieves 1.399.

## 7 Conclusion

In this paper, we tackled the problem of generating diverse and admissible predictions by understanding each agent’s multimodal context. We proposed a model that learns agent-to-agent interactions and agent-to-scene interactions using attention mechanisms, resulting in better prediction in terms of precision, diversity, and admissibility. We also developed a new approximation method that provides richer information about the true trajectory distribution and allows more accurate training of flow-based generative models. Finally, we present new metrics that provide a holistic view of the quantity and the quality of diversity in prediction, and a NUSCENES trajectory extraction code to support future research in diverse and admissible trajectory forecasting.

## References

1. Alahi, A., Goel, K., Ramanathan, V., Robicquet, A., Fei-Fei, L., Savarese, S.: Social lstm: Human trajectory prediction in crowded spaces. In: Proceedings of the IEEE conference on computer vision and pattern recognition. pp. 961–971 (2016)
2. Ayhan, S., Samet, H.: Aircraft trajectory prediction made easy with predictive analytics. In: Proceedings of the 22nd ACM SIGKDD International Conference on Knowledge Discovery and Data Mining. pp. 21–30 (2016)
3. Bansal, M., Krizhevsky, A., Ogale, A.: Chauffeurnet: Learning to drive by imitating the best and synthesizing the worst. arXiv preprint arXiv:1812.03079 (2018)
4. Bernstein, D.S., So, W.: Some explicit formulas for the matrix exponential. IEEE Transactions on Automatic Control **38**(8), 1228–1232 (1993)
5. Borkowski, P.: The ship movement trajectory prediction algorithm using navigational data fusion. Sensors **17**(6), 1432 (2017)
6. Caesar, H., Bankiti, V., Lang, A.H., Vora, S., Liong, V.E., Xu, Q., Krishnan, A., Pan, Y., Baldan, G., Beijbom, O.: nuscenes: A multimodal dataset for autonomous driving. arXiv preprint arXiv:1903.11027 (2019)
7. Casas, S., Luo, W., Urtasun, R.: Intentnet: Learning to predict intention from raw sensor data. In: Conference on Robot Learning. pp. 947–956 (2018)
8. Chang, M.F., Lambert, J., Sangkloy, P., Singh, J., Bak, S., Hartnett, A., Wang, D., Carr, P., Lucey, S., Ramanan, D., et al.: Argoverse: 3d tracking and forecasting with rich maps. In: Proceedings of the IEEE Conference on Computer Vision and Pattern Recognition. pp. 8748–8757 (2019)
9. Deo, N., Trivedi, M.M.: Convolutional social pooling for vehicle trajectory prediction. In: Proceedings of the IEEE Conference on Computer Vision and Pattern Recognition Workshops. pp. 1468–1476 (2018)
10. Djuric, N., Radosavljevic, V., Cui, H., Nguyen, T., Chou, F.C., Lin, T.H., Schneider, J.: Short-term motion prediction of traffic actors for autonomous driving using deep convolutional networks. arXiv preprint arXiv:1808.05819 (2018)
11. Felsen, P., Lucey, P., Ganguly, S.: Where will they go? predicting fine-grained adversarial multi-agent motion using conditional variational autoencoders. In: Proceedings of the European Conference on Computer Vision (ECCV). pp. 732–747 (2018)
12. Fernando, T., Denman, S., Sridharan, S., Fookes, C.: Soft + hardwired attention: An LSTM framework for human trajectory prediction and abnormal event detection. CoRR **abs/1702.05552** (2017), <http://arxiv.org/abs/1702.05552>
13. Goodfellow, I., Pouget-Abadie, J., Mirza, M., Xu, B., Warde-Farley, D., Ozair, S., Courville, A., Bengio, Y.: Generative adversarial nets. In: Advances in neural information processing systems. pp. 2672–2680 (2014)

14. Gupta, A., Johnson, J., Fei-Fei, L., Savarese, S., Alahi, A.: Social gan: Socially acceptable trajectories with generative adversarial networks. In: Proceedings of the IEEE Conference on Computer Vision and Pattern Recognition. pp. 2255–2264 (2018)
15. Kim, B., Kang, C.M., Kim, J., Lee, S.H., Chung, C.C., Choi, J.W.: Probabilistic vehicle trajectory prediction over occupancy grid map via recurrent neural network. In: 2017 IEEE 20th International Conference on Intelligent Transportation Systems (ITSC). pp. 399–404. IEEE (2017)
16. Kingma, D.P., Ba, J.: Adam: A method for stochastic optimization. arXiv preprint arXiv:1412.6980 (2014)
17. Kingma, D.P., Salimans, T., Jozefowicz, R., Chen, X., Sutskever, I., Welling, M.: Improved variational inference with inverse autoregressive flow. In: Advances in neural information processing systems. pp. 4743–4751 (2016)
18. Krajewski, R., Bock, J., Kloeker, L., Eckstein, L.: The highd dataset: A drone dataset of naturalistic vehicle trajectories on german highways for validation of highly automated driving systems. In: 2018 21st International Conference on Intelligent Transportation Systems (ITSC). pp. 2118–2125. IEEE (2018)
19. Lee, N., Choi, W., Vernaza, P., Choy, C.B., Torr, P.H., Chandraker, M.: Desire: Distant future prediction in dynamic scenes with interacting agents. In: Proceedings of the IEEE Conference on Computer Vision and Pattern Recognition. pp. 336–345 (2017)
20. Liang, P.P., Lim, Y.C., Tsai, Y.H.H., Salakhutdinov, R., Morency, L.P.: Strong and simple baselines for multimodal utterance embeddings. In: Proceedings of the 2019 Conference of the North American Chapter of the Association for Computational Linguistics: Human Language Technologies, Volume 1 (Long and Short Papers) (2019)
21. Ma, Y., Zhu, X., Zhang, S., Yang, R., Wang, W., Manocha, D.: Trafficpredict: Trajectory prediction for heterogeneous traffic-agents. In: Proceedings of the AAAI Conference on Artificial Intelligence. vol. 33, pp. 6120–6127 (2019)
22. Park, S.H., Kim, B., Kang, C.M., Chung, C.C., Choi, J.W.: Sequence-to-sequence prediction of vehicle trajectory via lstm encoder-decoder architecture. In: 2018 IEEE Intelligent Vehicles Symposium (IV). pp. 1672–1678. IEEE (2018)
23. Paszke, A., Gross, S., Chintala, S., Chanan, G., Yang, E., DeVito, Z., Lin, Z., Desmaison, A., Antiga, L., Lerer, A.: Automatic differentiation in pytorch. In: NIPS-W (2017)
24. Pham, H., Liang, P.P., Manzini, T., Morency, L., Póczos, B.: Found in translation: Learning robust joint representations by cyclic translations between modalities. In: The Thirty-Third AAAI Conference on Artificial Intelligence, AAAI 2019 (2019)
25. Qureshi, A.H., Nakamura, Y., Yoshikawa, Y., Ishiguro, H.: Show, attend and interact: Perceivable human-robot social interaction through neural attention q-network. In: 2017 IEEE International Conference on Robotics and Automation (ICRA). pp. 1639–1645. IEEE (2017)
26. Rezende, D.J., Mohamed, S.: Variational inference with normalizing flows. arXiv preprint arXiv:1505.05770 (2015)
27. Rhinehart, N., Kitani, K.M., Vernaza, P.: R2p2: A reparameterized pushforward policy for diverse, precise generative path forecasting. In: Proceedings of the European Conference on Computer Vision (ECCV). pp. 772–788 (2018)
28. Rhinehart, N., McAllister, R., Kitani, K., Levine, S.: Precog: Prediction conditioned on goals in visual multi-agent settings. In: Proceedings of the IEEE International Conference on Computer Vision. pp. 2821–2830 (2019)
29. Rodriguez, C., Fernando, B., Li, H.: Action anticipation by predicting future dynamic images. In: Proceedings of the European Conference on Computer Vision (ECCV). pp. 0–0 (2018)

30. Rudenko, A., Palmieri, L., Herman, M., Kitani, K.M., Gavrila, D.M., Arras, K.O.: Human motion trajectory prediction: A survey. arXiv preprint arXiv:1905.06113 (2019)
31. Sadeghian, A., Kosaraju, V., Sadeghian, A., Hirose, N., Rezatofghi, H., Savarese, S.: Sophie: An attentive gan for predicting paths compliant to social and physical constraints. In: Proceedings of the IEEE Conference on Computer Vision and Pattern Recognition. pp. 1349–1358 (2019)
32. Shapiro, I.I.: The prediction of satellite orbits. In: Dynamics of Satellites/Dynamique des Satellites, pp. 257–312. Springer (1963)
33. Sun, C., Karlsson, P., Wu, J., Tenenbaum, J.B., Murphy, K.: Stochastic prediction of multi-agent interactions from partial observations. arXiv preprint arXiv:1902.09641 (2019)
34. Sutskever, I., Vinyals, O., Le, Q.: Sequence to sequence learning with neural networks. *Advances in Neural Information Processing Systems* **4** (09 2014)
35. Tang, C., Salakhutdinov, R.R.: Multiple futures prediction. In: *Advances in Neural Information Processing Systems*. pp. 15398–15408 (2019)
36. Vaswani, A., Shazeer, N., Parmar, N., Uszkoreit, J., Jones, L., Gomez, A.N., Kaiser, L., Polosukhin, I.: Attention is all you need. In: *Advances in neural information processing systems*. pp. 5998–6008 (2017)
37. Vemula, A., Muelling, K., Oh, J.: Social attention: Modeling attention in human crowds. In: 2018 IEEE international Conference on Robotics and Automation (ICRA). pp. 1–7. IEEE (2018)
38. Verlet, L.: Computer” experiments” on classical fluids. i. thermodynamical properties of lennard-jones molecules. *Physical review* **159**(1), 98 (1967)
39. Xu, K., Ba, J., Kiros, R., Cho, K., Courville, A., Salakhudinov, R., Zemel, R., Bengio, Y.: Show, attend and tell: Neural image caption generation with visual attention. In: *International conference on machine learning*. pp. 2048–2057 (2015)
40. Zhao, T., Xu, Y., Monfort, M., Choi, W., Baker, C., Zhao, Y., Wang, Y., Wu, Y.N.: Multi-agent tensor fusion for contextual trajectory prediction. In: *Proceedings of the IEEE Conference on Computer Vision and Pattern Recognition*. pp. 12126–12134 (2019)